Temperature dependence of the optical properties in GaMnN

L. L. Guo, W. Z. Shen,[a] and Y. H. Zhang
Laboratory of Condensed Matter Spectroscopy and Opto-Electronic Physics, Department of Physics, Shanghai Jiao Tong University, 1954 Hua Shan Road, Shanghai 200030, People's Republic of China

(Received 26 September 2005; accepted 7 April 2006; published online 15 June 2006)

Temperature-dependent transmission measurements are carried out on ion-implanted GaMnN with different Mn-implantation doses. With a detailed procedure developed for analyzing the transmission spectra, we obtain the temperature effects in optical properties of GaMnN (including GaN), such as absorption coefficient, band gap, Urbach band tail characteristics, refractive index, and extinction coefficient. Two sets of temperature- and photon energy-dependent empirical formulas are established, which not only unify the various experimental data reported in the literature, but also provide an experimental database of optical properties in GaMnN. Furthermore, we reveal that the dependence of these optical properties on the Mn-implantation doses is closely related to the impact of Mn on the crystal structure. © *2006 American Institute of Physics*.
[DOI: 10.1063/1.2203427]

I. INTRODUCTION

Diluted magnetic semiconductors (DMS) have recently attracted considerable attention for creating a class of "spintronic" semiconductor devices with unprecedented functionality,[1–4] such as spin-field-effect transistors, spin-light-emitting diodes, spin-resonant tunneling device, and electrically controlled magnetic sensors and actuators. Particularly, GaMnN is a very promising material as a candidate of DMS, since many groups have predicted theoretically[5] and validated experimentally[6–9] that the Curie temperature (T_C) of GaMnN exceeds room temperature. A variety of methods have been reported to synthesize single-phase GaMnN, including diffusion,[6] ion implantation,[10] ammonothermal,[11] as well as epitaxial growth by molecular-beam epitaxy (MBE),[7] hydride vapor-phase epitaxy[8] (HVPE), and metal-organic chemical-vapor deposition (MOCVD).[9] So far, a great deal of emphasis has been placed on the origin of the ferromagnetic behavior in GaMnN. Kronik *et al.*[12] have predicted theoretically that the ferromagnetic properties are related to the occupancy of Mn energy band and the position of the Fermi level related to this band, while relating experimental work is currently under way to understand the mechanism of the ferromagnetism.[9]

Besides the magnetic characteristics, another crucial step towards the realization of GaMnN-based devices is to clearly understand the structural, optical, and electrical properties of GaMnN, especially the Mn related phenomenon. X-ray diffraction (XRD), transmission electron microscopy, and extended x-ray-absorption fine-structure measurements have been employed to examine the effects of Mn doping on structural properties, and to determine whether Mn substituted for Ga on lattice positions or presented as Mn clusters.[13–15] Optical studies on GaMnN have been widely concerned, but up-to-date optical properties are still limited and deficient. Photoluminescence (PL) investigation has been carried out on the Mn-related emission characteristics in GaMnN.[16,17] However, in order to present obvious emission peaks, PL has to be measured at a relatively low temperature especially for ion-implanted GaMnN, which leads to the difficulty in obtaining the temperature dependence of optical properties. Optical transmission/reflectance measurements have been performed on GaMnN,[18–20] but, without detailed theoretical analysis, unambiguous optical properties cannot be yielded directly from the optical spectra due to the poor absorption edge of GaMnN. In addition, only a few electrical properties, such as sheet resistivity and capacitance, has been reported for GaMnN, and most of the data obtained indicate that it is either insulating or *n* type.[18,21]

In this paper, by the aid of detailed analyses of structural characteristics, we present a comprehensive experimental and theoretical transmission study, which not only provides much more reliable and overall optical properties for ion-implanted GaMnN, but also addresses the dependence of these optical properties on the Mn-implantation doses. We further provide an experimental database of optical properties in GaMnN by establishing two sets of temperature- and photon energy-dependent empirical formulas for absorption coefficient, band gap, Urbach band tail, and refractive index.

II. EXPERIMENTAL DETAILS

We employ the high-quality Si-doped GaN thin film from Technologies and Devices International, Inc. The hexagonal GaN epilayer with a thickness of 3.8 μm was grown on (0001) sapphire substrate by HVPE. Hall measurement shows *n*-type carrier concentration of 1.5×10^{18} cm^{-3} at room temperature. The as-grown sample was then scribed and cut into ten pieces, which are equivalent in size (1×1 cm^2). Every two pieces, as a group, were uniformly implanted with the same Mn dose at a constant energy of 190 keV. We selected five Mn-implantation doses of 1×10^{16}, 3×10^{16}, 5×10^{16}, 7×10^{16}, and 9×10^{16} cm^{-2} for the five groups, corresponding to about 1%, 3%, 5%, 7%, and 9% Mn concentration in the implanted GaMnN region,

[a]Author to whom correspondence should be addressed; electronic mail: wzshen@sjtu.edu.cn

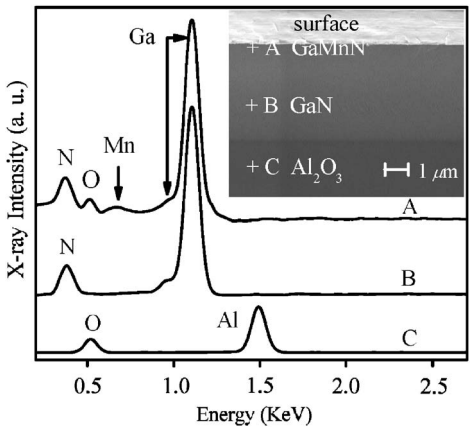

FIG. 1. EDX spectra taken on different points of A, B, and C within a typical RTA GaMnN sample (3×10^{16} cm^{-2} Mn). Shown in the inset are the corresponding positions in the SEM cross-section image, where points A, B, and C represent the layers of GaMnN, GaN, and sapphire substrate, respectively.

respectively.[18] To avoid amorphization, the samples were held at a temperature of 350 °C during the implantation process. The estimated depth of the implanted layer was about 150 nm from the sample surface.[16] After implantation, rapid thermal annealing (RTA) was carried out on one piece of each group at 900 °C for 1 min, in a flowing N_2 atmosphere with implanted area facing down.

In order to confirm the three-layer structure (GaMnN/GaN/sapphire) in our samples, we performed the scanning electron micrograph (SEM) and energy dispersive x-ray (EDX) spectrometry (Philips XL30FEG) measurements. Figure 1 displays the EDX spectra taken on different layers of a typical RTA GaMnN sample (3×10^{16} cm^{-2} Mn) with the SEM cross-section image shown in the inset. Clear Al and O peaks can be seen in the EDX spectrum of the bottom sapphire substrate. In the surface epilayer (EDX detection point A), a well-resolved Mn peak is observed, in addition to the structures of Ga, N, and O (due to the surface oxidation[16]). In contrast, only strong peaks of Ga and N are revealed in the inner epilayer. These EDX results clearly demonstrate that a thin GaMnN surface layer has been formed in the GaN epilayer after the Mn implantation. Furthermore, the crystal structure of GaMnN was checked by XRD measurements (Bruker AXS D8 Discover GADDS with a Cr K_α line), and the temperature-dependent ultraviolet transmission spectra were yielded through a Jobin Yvon 460 monochromator, in conjunction with a Janis variable temperature (10–300 K) closed-cycle refrigerator system.

III. THEORETICAL MODEL

In modeling the transmission spectra of the three-layer samples, we consider the multiple reflections at three interfaces: air to GaMnN layer (thickness d_{GaMnN}) (subscript 1), GaMnN layer to GaN layer (thickness d_{GaN}) (subscript 2), and GaN layer to sapphire substrate (subscript 3). The transmission for light passing through these samples can then be calculated using

$$T_{1,3}=\frac{(1-R_1)(1-L)T_{2,3}a_1}{1-R_1(1-L)R_{2,3}a_1^2}, \tag{1}$$

with

$$T_{2,3}=\frac{(1-R_2)(1-R_3)a_2}{1-R_2R_3a_2^2},$$

$$R_{2,3}=R_2+\frac{R_3(1-R_2)^2a_2^2}{1-R_2R_3a_2^2},$$

$$a_1=\exp(-\alpha_{\mathrm{GaMnN}}d_{\mathrm{GaMnN}}),$$

$$a_2=\exp(-\alpha_{\mathrm{GaN}}d_{\mathrm{GaN}}).$$

The parameter L indicates the fraction of light loss at the epilayer surface and is treated as a variable parameter to match the calculated transmission to the measured transmission. R_1, R_2, and R_3 are the reflectivities at the three interfaces, respectively, and can be obtained from

$$R=\frac{(n_i-n_j)^2}{(n_i+n_j)^2}. \tag{2}$$

The refractive index n of GaMnN (including GaN) is a function of both wavelength and temperature, which can be obtained from the theoretical calculation using a modified model dielectric function of Kawashima *et al.*,[22] with terms attributed to the transitions at four lowest critical points (E_0, E_{1A}, E_{1B}, and E_{1C} for hexagonal materials). Assuming the valence and conduction bands are parabolic and using the Kramers-Kronig transformation (KKT), the contribution of the E_0 gap is given by

$$\varepsilon_0(E)=AE_0^{-3/2}\chi_0^{-2}[2-(1+\chi_0)^{1/2}-(1-\chi_0)^{1/2}],$$
$$\chi_0=\frac{E+i\Gamma_0}{E_0}, \tag{3}$$

where A and Γ_0 are the strength and damping constants of the E_0 transition, respectively. The exciton contributions at E_0 critical point can be simply written, with Lorentzian line shape, as

$$\varepsilon_{0X}(E)=\sum_{m=1}^{\infty}\frac{A_0^{\mathrm{ex}}}{m^3}\frac{1}{E_0-(G_0^{3D}/m^2)-E-i\Gamma_0}, \tag{4}$$

where A_0^{ex} is the three-dimensional (3D) exciton strength parameter, and G_0^{3D} is the 3D exciton binding energy. Contributions of the two-dimensional (2D) M_0 critical points $E_{1\beta}(\beta=\mathrm{A},\mathrm{B},\mathrm{C})$ are given by

$$\varepsilon_1(E)=-\sum_{\beta=\mathrm{A,B,C}}B_{1\beta}\chi_{1\beta}^{-2}\ln(1-\chi_{1\beta}^2),\quad \chi_{1\beta}=\frac{E+i\Gamma_{1\beta}}{E_{1\beta}}, \tag{5}$$

where $B_{1\beta}$ and $\Gamma_{1\beta}$ are the strengths and the damping constants of the $E_{1\beta}$ transitions, respectively. The contributions of 2D excitons can be written as

$$\varepsilon_{1X}(E) = \sum_{\beta=A,B,C} \sum_{m=1}^{\infty} \frac{B_{1\beta}^{X}}{(2m-1)^3} \frac{1}{E_{1\beta} - (G_{1\beta}^{2D}/(2m-1)^2) - E - i\Gamma_{1\beta}}, \quad (6)$$

where $B_{1\beta}^{X}$ and $G_{1\beta}^{2D}$ are the strengths and binding energies of the excitons at $E_{1\beta}$, respectively.

By combining Eqs. (3)–(6), the total dielectric function, with a real part $\varepsilon_r(E)$ and an imaginary part $\varepsilon_i(E)$, is then given by

$$\varepsilon(E) = \varepsilon_{1\infty} + \varepsilon_0(E) + \varepsilon_{0X}(E) + \varepsilon_1(E) + \varepsilon_{1X}(E) = \varepsilon_r(E) + i\varepsilon_i(E), \quad (7)$$

where $\varepsilon_{1\infty}$ is the dielectric constant arising from transitions outside the considered spectral range. Finally, the refractive index n and extinction coefficient k can be obtained as[23]

$$n(E) = \sqrt{\frac{[\varepsilon_r(E)^2 + \varepsilon_i(E)^2]^{1/2} + \varepsilon_r(E)}{2}}, \quad (8)$$

$$k(E) = \sqrt{\frac{[\varepsilon_r(E)^2 + \varepsilon_i(E)^2]^{1/2} - \varepsilon_r(E)}{2}}. \quad (9)$$

Including the Urbach exponential absorption edge and intrinsic square-root absorption, the absorption coefficient of GaMnN can be written as[24]

$$\alpha(E) = \begin{cases} \alpha_0 \exp[(E - E_e)/E_U], & E < E_g \\ \alpha_d (E - E_g')^{1/2}, & E \geq E_g, \end{cases} \quad (10)$$

where the physical origins of the above four band-gap parameters are as follows: E_e coincides roughly with the energy of the lowest free exciton energy at 0 K, E_g' is the band-gap energy of the material without band tail distortions, and E_U is the Urbach band tail parameter. These material parameters, including α_0 and α_d, are linked through the continuity at the energy band gap of E_g.

IV. RESULTS AND DISCUSSION

A. X-ray diffraction

We start with the quality and crystal structure of these GaMnN samples through XRD measurements. Figure 2 displays the XRD patterns and the c-plane lattice constants of (a) as-implanted and (b) RTA GaMnN samples with different Mn-implantation doses. It is found that only the peaks corresponding to the GaN (0002), $(10\bar{1}1)$, and $(10\bar{1}2)$ orientations were detected in all the XRD spectra. The absence of secondary phases of Ga_xMn_y indicates that the GaMnN layers without any phase separation have been realized. The c-plane lattice constant of GaMnN, determined from the (0002) peaks, is found to be larger than that of GaN, which has been reported in similar studies for GaN grown by HVPE,[8] MBE,[25] and MOCVD.[26] With the increase of Mn dose, the lattice constant decreases because of the incorporation of Mn substitutionally on the Ga sublattice. However, the lattice constant turns to increase as the Mn dose gained beyond 3×10^{16} cm^{-2}, which is due to the incorporation of interstitial Mn.[15] This kind of phenomenon has been observed in both the as-implanted and RTA GaMnN samples, suggesting that the maximum solubility for substitution Mn is around 3×10^{16} cm^{-2}, which is probably the optimal implantation dose for the GaMnN crystal structure. Similar results have also been reported by Thaler *et al.*[15]

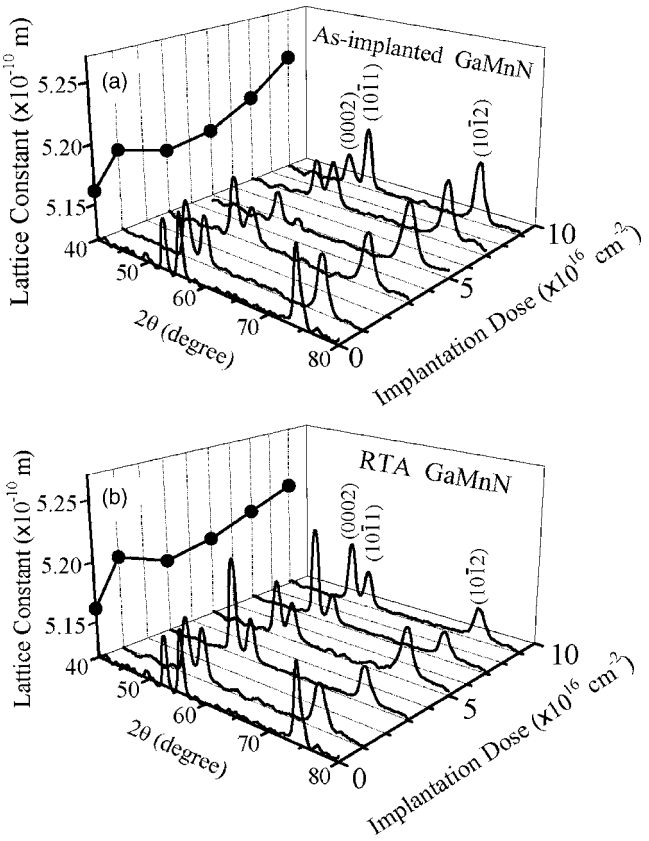

FIG. 2. XRD patterns (solid curves) and c-plane lattice constants (solid circles) of (a) as-implanted and (b) RTA GaMnN samples with different Mn-implantation doses (zero implantation dose represents the unimplanted GaN sample).

B. Transmission spectra

Now, we focus on the temperature-dependent transmission spectra of these GaMnN samples with different Mn-implantation doses for the detailed optical properties. Figure 3 shows the temperature-dependent spectra of (a) GaN and (b) RTA GaMnN (5×10^{16} cm^{-2} Mn) samples, together with the theoretical fitting results. It is clear that the transmission spectra of GaN show a sharp absorption edge, which has blueshift at lower temperature. In contrast, for GaMnN samples, the absorption edge becomes flat, though the temperature dependence is the same. This kind of change in absorption edge, also observed in Ref. 18, is related with the introduction of the lattice defect and disorder after Mn implantation. Figure 4 displays both the experimental and theoretical results of (a) as-implanted and (b) RTA GaMnN samples with different Mn doses at 10 K. We notice that, in comparison with the as-implanted GaMnN samples, the absorption edges rise up to a certain extent after RTA, indicating some kind of recovery in the GaMnN crystal structure. It should be noted that the theoretical results calculated from

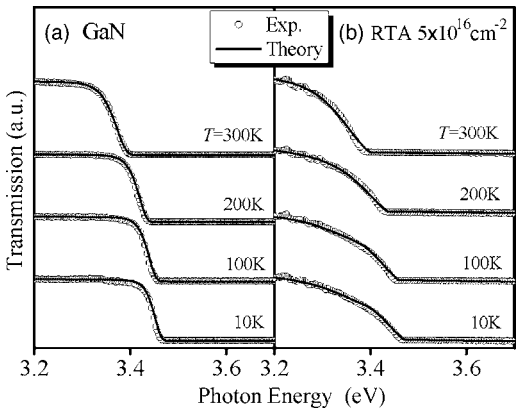

FIG. 3. Temperature-dependent experimental (open circles) and theoretical (solid curves) transmission spectra of (a) GaN and (b) RTA GaMnN (5×10^{16} cm^{-2} Mn).

Eqs. (1)–(10) fit the experimental data very well in both Figs. 3 and 4, with a GaMnN layer thickness d_{GaMnN} of 150 nm in the calculation. Through the calculations for the three-layer samples, we can extract and will show below the detailed temperature-dependent optical properties of GaMnN, such as the absorption coefficient α, band gap E_g, Urbach band tail parameter E_U, refractive index n, and extinction coefficient k.

C. Absorption coefficient

Figure 5 displays the yielded Urbach and intrinsic absorption coefficient (solid curves) of the GaN and RTA GaMnN at 300 K. It can be seen clearly that the Urbach exponential absorption and intrinsic square-root absorption are closely linked at the turning points α_g (the absorption coefficient at $E=E_g$). In addition, we note that the absorption coefficient above E_g in GaMnN is slightly larger than that of GaN, consistent with the observation by Polyakov *et al.* in Ref. 27. In order to demonstrate the reliability of the yielded absorption coefficient, we have also shown in Fig. 5 the reported results in the literature for a direct comparison: the room-temperature absorption coefficient near the band gap of GaMnN with different Mn concentrations in Refs. 27 (open circles) and 20 (open triangles). It is clear that our results are in reasonably good agreement with the data reported by different groups using different growth methods.

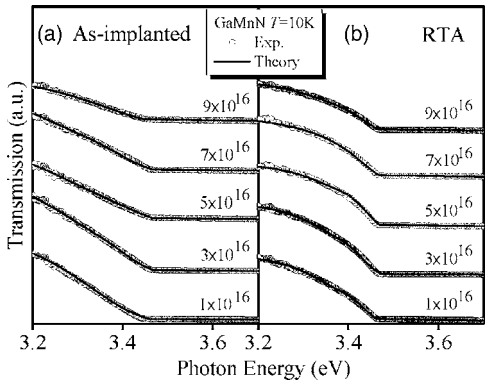

FIG. 4. Experimental (open circles) and theoretical (solid curves) transmission spectra of (a) as-implanted and (b) RTA GaMnN samples with different Mn-implantation doses at 10 K.

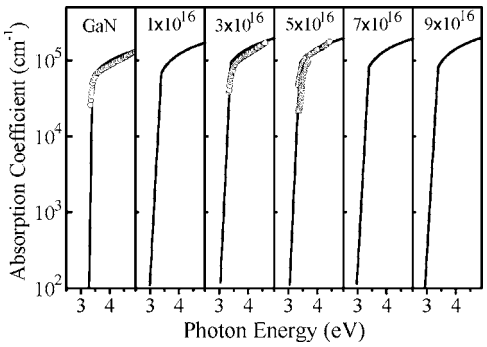

FIG. 5. The yielded Urbach and intrinsic absorption coefficient (solid curves) of the GaN and RTA GaMnN with different Mn-implantation doses at 300 K. The open circles and triangles are experimental data reported in Refs. 27 and 20 respectively.

We have further established an overall empirical base for the temperature- and photon energy-dependent absorption coefficient of GaMnN through the absorption and band-gap parameters in Eq. (10). The absorption parameters α_0 and α_d are usually independent of temperature and proportional to temperature in semiconductors, respectively.[28] In the case of GaMnN, the absorption parameter α_0 is also found to be a constant, while α_d does have a linear dependence on temperature. The temperature-dependent band-gap parameters E_g, E_e, and E_g' can be described well by the empirical Varshni equation. For the Urbach band tail parameter E_U, we have employed the temperature-dependent band tail theory discussed in Sec. IV E. As a result, the overall absorption coefficient of GaMnN can be described by Eq. (10) through the following empirical formulas:

$$
\begin{aligned}
&\alpha_d = \alpha_1 - \alpha_2 T \ \mathrm{cm}^{-1},\\
&\alpha_g = \alpha_0 \exp[(E_g - E_e)/E_U] \ \mathrm{cm}^{-1},\\
&E_g(T) = E_g(0) - \beta_1 T^2/(\beta_2 + T) \ \mathrm{eV},\\
&E_e(T) = E_e(0) - \beta_3 T^2/(\beta_4 + T) \ \mathrm{eV},\\
&E_g'(T) = E_g'(0) - \beta_5 T^2/(\beta_6 + T) \ \mathrm{eV},\\
&E_U(T) = E_U(0) + \beta_7 T^{3/2} + \beta_8 \coth \frac{529}{T} \ \mathrm{meV},
\end{aligned}
\tag{11}
$$

with the parameters in these formulas listed in Table I for different Mn-implantation doses.

D. Energy band gap

The transmission spectra in Fig. 3 have clearly revealed the decrease of energy band gap in GaMnN with the increase of temperature. However, the normally linear extrapolated method from transmission/absorption spectra is not very accurate for the determination of energy band gap, especially for the flat absorption edge case. Our above detailed calculation of the transmission spectra will yield more reliable and precise band gap E_g than that from the normally linear extrapolated method. Figure 6 displays the obtained temperature-dependent band gap E_g (open circles), together

TABLE I. Parameters for the set of empirical formulas [Eq. (11)] to describe the temperature-dependent absorption coefficient, band gap, and Urbach band tail in both the as-implanted and RTA GaMnN (including GaN) with different Mn-implantation doses.

		α_d (cm^{-1})			E_g (eV)			E_c (eV)			E_g (eV)			E_U (meV)		
Samples		α_0 (10^4 cm^{-1})	α_1 (10^5 cm^{-1})	α_2 (cm^{-1} /K)	$E_g(0)$ (eV)	β_1 (10^{-4} eV/K)	$\beta 2$ (K)	$E_e(0)$ (eV)	β_3 (10^{-4} eV/K)	β_4 (K)	$E'_g(0)$ (eV)	β_5 (10^{-4} eV/K)	β_6 (K)	$E_U(0)$ (meV)	β_7 (10^{-4} $meV/T^{3/2}$)	β_8 (meV)
GaN		3.7	2.20	220	3.478	7.1	621	3.470	6.9	621	3.378	7.5	621	11.5	13.5	0.724
As-implanted GaMnN ($\times 10^{16}$ cm^{-2})	1	2.8	1.30	150	3.460	7.1	785	3.360	8.7	785	3.172	9.8	420	114.2	0	0
	3	3.3	1.46	200	3.468	7.1	718	3.388	7.1	718	3.199	7.9	580	95.5	0	0
	5	3.8	1.45	160	3.466	7.1	604	3.381	6.5	875	3.177	9.5	560	119.3	0	0
	7	3.7	1.56	170	3.465	7.1	704	3.363	6.3	704	3.099	7.8	580	124.8	0	0
	9	3.6	1.46	140	3.448	7.1	845	3.298	7.1	845	3.067	8.0	580	132.8	0	0
RTA GaMnN ($\times 10^{16}$ cm^{-2})	1	2.8	1.30	150	3.461	7.1	670	3.413	7.8	670	3.240	9.5	550	57.5	3.80	2.91
	3	3.3	1.46	200	3.475	7.1	609	3.439	7.2	609	3.282	7.1	609	48.5	6.16	2.97
	5	3.8	1.45	160	3.470	7.1	634	3.438	7.6	634	3.236	9.6	480	49.0	5.37	1.92
	7	3.7	1.46	140	3.469	7.1	562	3.426	7.8	562	3.180	9.8	432	59.0	3.77	2.69
	9	3.6	1.46	140	3.467	7.1	591	3.417	7.4	591	3.154	8.6	591	61.5	6.96	3.40

with the empirical Varshni fitting of Eq. (11) (solid curves with the fitting parameters listed in Table I), of (a) as-implanted and (b) RTA GaMnN samples with different Mn-implantation doses. We note that the yielded parameters of 0.71 meV/K and 621 K for GaN on sapphire substrate are very close to those tabulated data of 0.72 meV/K and 600 K (Ref. 29) (see the solid circles in Fig. 6 for comparison). Equation (11) and Table I have also given the temperature dependence of the other two band-gap parameters of E_e and E'_g, which have the same variation law as the energy band gap E_g.

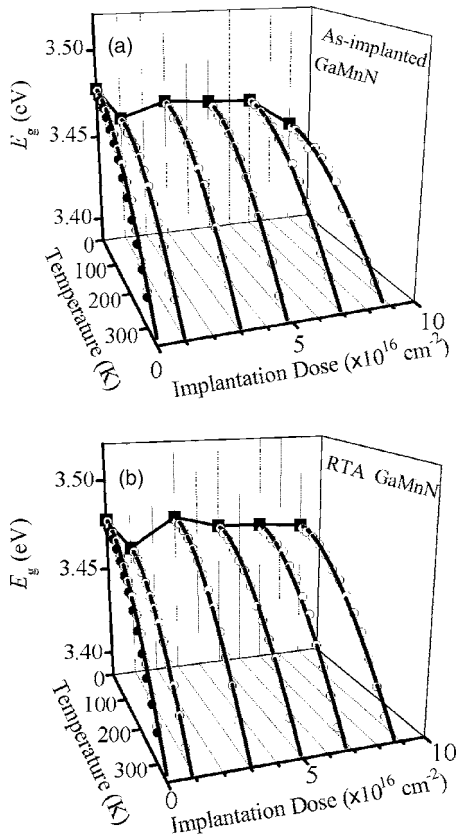

FIG. 6. The yielded temperature-dependent band gap E_g (open circles), together with the empirical Varshni fitting of Eq. (11) (solid curves), of (a) as-implanted and (b) RTA GaMnN samples (including GaN). The band gap at 0 K [$E_g(0)$] obtained from Eq. (11) is shown as solid squares. The solid circles are experimental results of GaN on sapphire substrate reported in Ref. 29.

In order to investigate the effect of Mn-implantation dose on E_g, we have also shown the band gap at 0 K [$E_g(0)$] as solid squares in Fig. 6. Comparing with GaN, it is clear that a small redshift (3–30 meV) in the band gap can be observed in both the as-implanted and RTA GaMnN samples. Polyakov *et al.*[18] have reported an obvious redshift in the absorption edge of the Mn-implanted GaN samples, but have not given the detailed redshift data. The flat absorption edge of GaMnN might be their difficulty in determining the precise values of E_g, indicating the necessity of our present theoretical work. Reference 19 has also reported an estimated redshift of 30 meV in their 1.5×10^{21} cm^{-3} Mn-doped GaN sample. In comparison with the variation of lattice constant with the Mn-implantation dose shown in Fig. 2, the modification of energy band structure in GaMnN can be easily attributed to the change of the lattice constant. The overall increase of the lattice constant due to the Mn-implantation corresponds well to the decrease of the energy band gap. The decrease of lattice constant, due to the incorporation of Mn substitutionally on the Ga sublattice, results in the increase of energy band gap, while the gradual increase of the lattice constant, due to the incorporation of interstitial Mn, leads to the decrease of E_g.

E. Urbach band tail

The temperature-dependent band tail parameter in GaMnN has also been analyzed by the recently proposed band tail theory of Shen *et al.*,[30] which is based on the calculation of density of occupied states and carrier-phonon in-

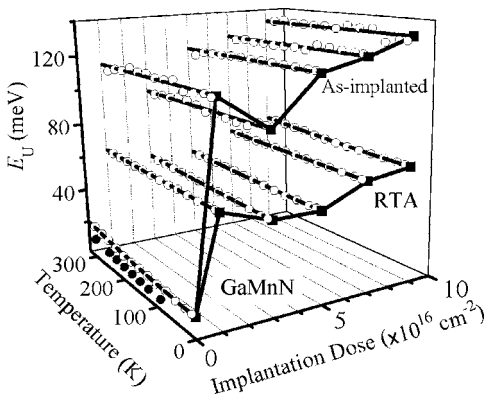

FIG. 7. The yielded temperature-dependent Urbach band tail E_U (open circles), together with the theoretical band tail fitting of Eq. (11) (solid curves), of as-implanted and RTA GaMnN samples (including GaN). The band tail at 0 K $[E_U(0)]$ obtained from Eq. (11) is shown as solid squares. The solid circles are experimental results of undoped GaN reported in Ref. 32.

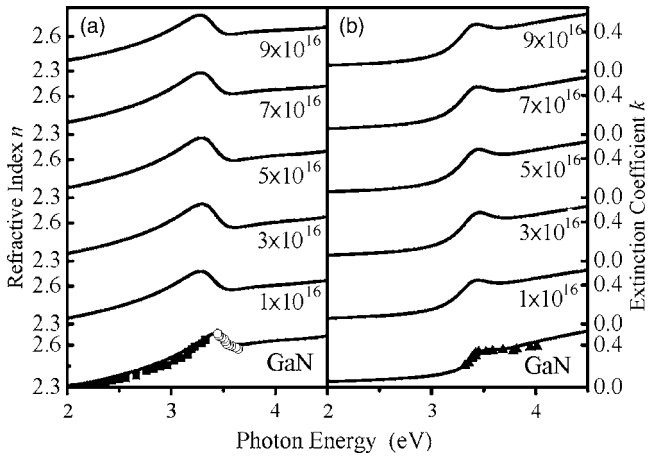

FIG. 8. The yielded (a) refractive index n and (b) extinction coefficient k of GaN and RTA GaMnN samples at 300 K. Also shown for comparison is the reported refractive index of GaN in Refs. 33 (solid squares) and 34 (open circles), as well as the extinction coefficient in Ref. 22 (solid triangles).

teraction in the adiabatic approximation. A quantitatively analytical formulation for the band tail parameter E_U can be deduced by taking three parts into account, including structural disorder, carrier-impurity interaction (mainly depends on carrier concentration and implicitly depends on temperature), and carrier-phonon interaction (mainly depends on temperature), which has the form of[30]

$$E_U(T) = \frac{1}{2}k_B U\theta_D + \frac{4\pi^2 Z^2 q^4 m^* L_D^3}{9\sqrt{3}\varepsilon^2\hbar^2}[(1-1/e)n_d + N_{BD}] + F\coth\left(\frac{\hbar\omega_{LO}}{2k_B T}\right), \quad (12)$$

with k_B the Boltzmann constant, U the lattice strain related with the structural disorder, θ_D the Debye temperature, Z the impurity charge, q the electron charge, m^* the carrier effective mass, ε the static dielectric permittivity, $\hbar$ the Planck's constant divided by 2π, n_d the carrier concentration difference between the center n_0 and the surface of the grain (the grain boundary contribution), N_{BD} the effective trap charge distribution (the grain defect contribution), F a constant, and $\hbar\omega_{LO}$ [=734 cm^{-1} (Ref. 31)] the longitudinal-optical (LO) phonon energy in GaN (the thermal contribution). The Debye length L_D is given by

$$L_D = \left(\frac{\varepsilon k_B T}{q^2 n_0}\right)^{1/2}. \quad (13)$$

The first term in the right-hand side of Eq. (12) is due to the contribution of structural disorder, which is independent of temperature, carrier concentration, and impurity concentration, and therefore is a constant for materials grown under the same growth conditions. The last equation of Eq. (11) is the simplified temperature dependent E_U of Eq. (12).

Figure 7 displays the obtained temperature-dependent band tail E_U (open circles), together with the theoretical fitting of Eq. (12) (solid curves with the fitting parameters listed in Table I), of both the as-implanted and RTA GaMnN samples with different Mn-implantation doses. Comparing with the reported E_U (solid circles) of undoped GaN in Ref. 32, our yielded E_U shows the similar temperature dependence, with the slightly large values (12–20 meV vs 6–14 meV) due to our Si doping case. It can be clearly seen that, after Mn-implantation, there is a rapid increase in E_U due to the formation of lattice defect and disorder in the crystal structure. No obvious temperature dependence of E_U can even be observed in as-implanted GaMnN, indicating that the contribution of structural disorder dominates over the other two interactions. After the treatment of RTA to recover some of lattice defect and structural disorder, E_U returns to low energy obviously, accompanying with obvious temperature dependence similar to that of GaN (also see Table I). Furthermore, the dependence of the band tail at 0 K $[E_U(0)]$ (solid squares) on the Mn-implantation dose also displays the closely related behavior with that of lattice constant in Fig. 2 and energy band gap in Fig. 6, except for the significant enhancement between GaMnN and GaN, due to the key role of lattice defect and disorder in E_U. The replacement of Mn with Ga site will release the structure disorder, resulting in the decrease of E_U, in contrast to the interstitial Mn case where reverse effect occurs.

F. Refractive index

Finally, we present in Fig. 8 the yielded photon energy dependence of (a) refractive index n and (b) extinction coefficient k of GaMnN (including GaN) with different Mn-implantation doses at 300 K. A peak can be clearly observed in every refractive index/extinction coefficient spectrum. The detailed KKT analysis in Ref. 28 has explained the appearance of these peaks in semiconductors, whose energy positions correspond approximately to the energy band gaps. As a result, the refractive index peak position shifts with Mn-implantation doses in GaMnN, displaying the closely related behavior with the energy band gap. At photon energies well above the band gap, the refractive index increases with photon energy, which is due to higher-lying-gap transitions.[28] Furthermore, we have also listed in Fig. 8 the reported data of n, k in GaN for a direct comparison: the refractive index in Refs. 33 (solid squares) and 34 (open circles), as well as the extinction coefficient in Ref. 22 (solid triangles). Good

TABLE II. Parameters for the empirical Sellmeier equation [Eqs. (14) and (15)] to describe the temperature-dependent refractive index n below the band gap of both the as-implanted and RTA GaMnN (including GaN) with different Mn-implantation doses.

		As-implanted GaMnN ($\times 10^{16}$ cm^{-2})					RTA GaMnN ($\times 10^{16}$ cm^{-2})				
Samples	GaN	1	3	5	7	9	1	3	5	7	9
γ_1	3.456	3.915	3.781	3.765	3.764	3.820	3.667	3.394	3.555	3.554	3.582
η_1 (10^{-3}/K)	1.570	1.660	1.700	1.360	1.690	2.500	1.560	0.819	1.020	1.390	0.939
γ_2	1.707	1.332	1.427	1.381	1.452	1.413	1.496	1.670	1.597	1.585	1.586
η_2 (10^{-3}/K)	1.620	1.610	1.670	1.290	1.670	2.270	1.420	0.981	1.070	1.450	1.230
γ_3	0.282	0.314	0.306	0.309	0.306	0.311	0.303	0.295	0.296	0.300	0.302
η_3 (10^{-5}/K)	6.042	6.757	6.620	6.300	6.900	7.733	4.134	4.357	3.559	5.807	6.603

agreement has been reached between the reported data and our yielded values, demonstrating further the reliability of our GaMnN results.

In order to summarize the temperature- and wavelength-dependent refractive index characteristics in GaMnN, we find that they can be described well by an empirical Sellmeier equation through fitting the experimental data below the band gap,

$$n(\lambda,T)^2 = m_1 + m_2/[1-(m_3/\lambda)^2], \tag{14}$$

where m_1, m_2, and m_3 are the fitting parameters, which depend on temperature T, and λ is the wavelength in micrometers. The best fit yields

$$\begin{aligned} m_1 &= \gamma_1 - \eta_1 T, \\ m_2 &= \gamma_2 - \eta_2 T, \\ m_3 &= \gamma_3 - \eta_3 T, \end{aligned} \tag{15}$$

with the parameters in these formulas listed in Table II for different Mn-implantation doses.

By the aid of the empirical formulas Eqs. (14) and (15), we can obtain the refractive index as a function of temperature and wavelength for GaMnN below the band gap, as well as the rate of refractive index change with temperature dn/dT. Shown in Fig. 9 is the temperature-dependent refractive index of GaN and RTA GaMnN at photon energy of 2.5 eV. The open circles are the experimental data from our detailed calculation of the transmission spectra, and the solid curves are the calculated results from the above Sellmeier equation. It can be seen that all of the calculated results fit the yielded data very well. In addition, we also find that the refractive index has a positive temperature coefficient, i.e., an increase of 0.013 (0.014) at 2.5 eV with the temperature from 10 to 300 K in GaN (GaMnN, 3×10^{16} cm^{-2} Mn). The positive temperature coefficient, which can also be understood by the KKT analysis,[28] is related with the negative temperature dependence of the GaMnN energy band gap shown in Sec. IV D and Fig. 6. The resultant dn/dT of 4.48×10^{-5} K^{-1} in GaN is close to the reported value of 4.33×10^{-5} K^{-1} in Ref. 35. Furthermore, due to the closely related relationship with the energy band gap, the refractive index at 0 K [obtained from empirical formulas of Eqs. (14) and (15), and shown as the solid squares in Fig. 9] does display the same dependence on the Mn-implantation dose as that of the lattice constant in Fig. 2, energy band gap in Fig. 6, and Urbach band tail in Fig. 7.

V. CONCLUSIONS

In summary, a comprehensive experimental and theoretical transmission study is presented for both the as-implanted and RTA GaMnN samples. We have obtained the temperature effects in optical properties of GaMnN (including GaN), such as absorption coefficient, band gap, Urbach band tail parameter, refractive index, and extinction coefficient. The temperature and photon energy dependences of the absorption coefficient, band gap, and Urbach band tail parameter are described by a series of empirical formulas. The temperature dependence of the refractive index dispersion below the band gap is found to obey a Sellmeier equation. These two sets of empirical formulas not only unify the various experimental data reported in the literature, but also provide an experimental database of optical properties in GaMnN. Furthermore, we investigate the dependence of these optical properties on the Mn-implantation doses, which is found to be closely related with the structural characteristics. All these optical properties are essential for the realization of GaMnN-based devices.

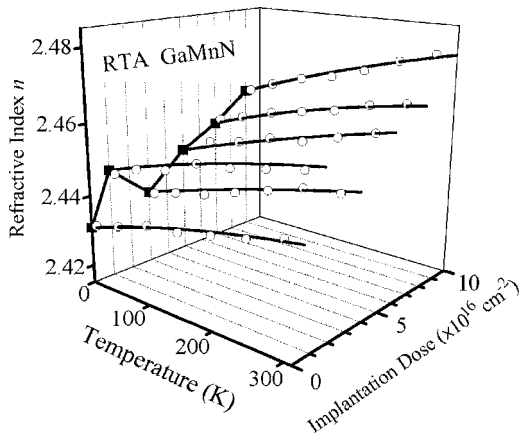

FIG. 9. Temperature-dependent refractive index of GaN and RTA GaMnN samples at a photon energy of 2.5 eV. The open circles are experimental data from our detailed calculation of the transmission spectra, and the solid curves are calculated results from the Sellmeier equation [Eqs. (14) and (15)]. The refractive index at 0 K obtained from the Sellmeier equation is shown as solid squares.

ACKNOWLEDGMENT

This work is supported in part by the National Natural Science Foundation of China under Contract Nos. 10125416, 10304010, and 60576067, as well as the National Minister of Education Program for Changjiang Scholars and Innovative Research Team in University (PCSIRT).

[1]H. Ohno, Science **281**, 951 (1998).
[2]G. A. Prinz, Science **282**, 1660 (1998).
[3]S. A. Wolf, D. D. Awschalom, R. A. Buhrman, J. M. Daughton, S. von Molnar, M. L. Roukes, A. Y. Chtchelkanova, and D. M. Treger, Science **294**, 1488 (2001).
[4]S. J. Pearton, C. R. Abernathy, D. P. Norton, A. F. Hebard, Y. D. Park, L. A. Boatner, and J. D. Budai, Mater. Sci. Eng., R. **40**, 137 (2003).
[5]T. Dietl, H. Ohno, F. Matsukura, J. Cibert, and D. Ferrand, Science **287**, 1019 (2000).
[6]M. L. Reed, N. A. El-Masry, H. H. Stadelmaier, M. K. Ritums, M. J. Reed, C. A. Parker, J. C. Roberts, and S. M. Bedair, Appl. Phys. Lett. **79**, 3473 (2001).
[7]G. T. Thaler *et al.*, Appl. Phys. Lett. **80**, 3964 (2002).
[8]Y. Y. Yu *et al.*, J. Cryst. Growth **269**, 270 (2004).
[9]M. J. Reed, F. E. Arkun, E. A. Berkman, N. A. Elmasry, J. Zavada, M. O. Luen, M. L. Reed, and S. M. Bedair, Appl. Phys. Lett. **86**, 102504 (2005).
[10]N. Theodoropoulou, A. F. Hebard, M. E. Overberg, C. R. Abernathy, S. J. Pearton, S. N. G. Chu, and R. G. Wilson, Appl. Phys. Lett. **78**, 3475 (2001).
[11]M. Zajac *et al.*, Appl. Phys. Lett. **78**, 1276 (2001).
[12]L. Kronik, M. Jain, and J. R. Chelikowsky, Phys. Rev. B **66**, 041203 (2002).
[13]S. Sonoda, T. Sasaki, Y. Yamamoto, S. Shimizu, K. Suga, and K. Kindo, Physica B **324**, 142 (2002).
[14]J. M. Baik, H. S. Kim, C. G. Park, and J. L. Lee, Appl. Phys. Lett. **83**, 2632 (2003).
[15]G. Thaler, R. Frazier, B. Gila, J. Stapleton, M. Davidson, C. R. Abernathy, S. J. Pearton, and C. Segre, Appl. Phys. Lett. **84**, 1314 (2004).
[16]Y. Shon, Y. H. Kwon, T. W. Kang, X. Fan, D. Fu, and Y. Kim, J. Cryst. Growth **245**, 193 (2002).
[17]I. T. Yoon, T. W. Kang, M. C. Jeong, M. H. Ham, and J. M. Myoung, Appl. Phys. Lett. **85**, 4878 (2004).
[18]A. Y. Polyakov, N. B. Smirnov, A. V. Govorkov, and N. Y. Pashkova, J. Appl. Phys. **92**, 3130 (2002).
[19]J. Xu *et al.*, Opt. Mater. (Amsterdam, Neth.) **23**, 163 (2003).
[20]S. S. A. Seo *et al.*, Appl. Phys. Lett. **82**, 4749 (2003).
[21]S. J. Pearton *et al.*, J. Phys.: Condens. Matter **16**, R209 (2004).
[22]T. Kawashima, H. Yoshikawa, S. Adachi, S. Fuke, and H. Ohtsuka, J. Appl. Phys. **82**, 3528 (1997).
[23]H. F. Yang, W. Z. Shen, and Q. J. Pang, J. Phys.: Condens. Matter **14**, 2067 (2002).
[24]W. Z. Shen, Int. J. Infrared Millim. Waves **23**, 61 (2002).
[25]Y. Cui and L. Li, Appl. Phys. Lett. **80**, 4139 (2002).
[26]M. C. Park, K. S. Huh, J. M. Myoung, J. M. Lee, J. Y. Chang, K. I. Lee, S. H. Han, and W. Y. Lee, Solid State Commun. **124**, 11 (2002).
[27]A. Y. Polyakov *et al.*, J. Appl. Phys. **92**, 4989 (2002).
[28]L. F. Jiang, W. Z. Shen, H. Ogawa, and Q. X. Guo, J. Appl. Phys. **94**, 5704 (2003).
[29]M. Ilegems, R. Dingle, and R. A. Logan, J. Appl. Phys. **43**, 3797 (1972).
[30]W. Z. Shen, L. F. Jiang, H. F. Yang, F. Y. Meng, H. Ogawa, and Q. X. Guo, Appl. Phys. Lett. **80**, 2063 (2002).
[31]W. Gebicki, J. Strzeszewski, G. Kamler, T. Szyszko, and S. Podsiadlo, Appl. Phys. Lett. **76**, 3870 (2000).
[32]S. Chichibu, T. Mizutani, T. Shioda, H. Nakanishi, T. Deguchi, T. Azuhata, T. Sota, and S. Nakamura, Appl. Phys. Lett. **70**, 3440 (1997).
[33]M. E. Lin, B. N. Sverdlov, S. Strite, H. Morkoc, and A. E. Drakin, Electron. Lett. **29**, 1759 (1993).
[34]N. Antoine-Vincent *et al.*, J. Appl. Phys. **93**, 5222 (2003).
[35]L. Siozade, S. Colard, M. Mihailovic, J. Leymarie, A. Vasson, N. Grandjean, M. Leroux, and J. Massies, Phys. Status Solidi B **216**, 73 (1999).